First Principle Study on Lead-Free $CH_3NH_3GeI_3$ and $CH_3NH_3GeBr_3$ Perovskite solar cell using FHI-aims Code

H. Abdulsalam[1*] and G. Babaji[2]

[1]Department of Physics, Yobe State University, Damaturu P.M.B.1144, Yobe Nigeria
[2]Department of Physics, Bayero University, Kano P.M.B. 3011, Kano Nigeria

**Corresponding author E-mail*: ahassanabdulsalam@gmail.com

(Received 09 January 2019, Accepted 28 March 2019, Published 31 March 2019)

Abstract

An Ab-initio calculation in the framework of Density Functional Theory (DFT), as implemented in the FHI-aims package within Generalized Gradient Approximation (GGA) with the pbe parameterization was carried out in this work. Although methyl ammonium lead iodide ($CH_3NH_3PbI_3$) has proven to be an effective photovoltaic material, there remains a main concern about the toxicity of lead. An investigation into the possible replacement of $CH_3NH_3PbI_3$ with $CH_3NH_3GeI_3$ and $CH_3NH_3GeBr_3$ as the active layer in perovskite solar cell was carried out. The electronic band structure, band gap energy and dielectric constants were calculated for $CH_3NH_3GeI_3$ and $CH_3NH_3GeBr_3$. The effect of temperature on linear thermal expansion coefficient and temperature dependence of lattice constant were studied in the temperature range of 273 to 318 K. Band gap shift due to lattice expansion was also studied. The dielectric constants of these materials were also determined. The energy band gap calculated for $CH_3NH_3GeI_3$ and $CH_3NH_3GeBr_3$ at their respective equilibrium lattice constant are 1.606 and 1.925eV respectively. A numerical simulation with some of these materials as the active layer in a perovskite solar cell was performed using General-purpose Photovoltaic Device Model (GPVDM) and the conversion efficiency of the resulting solar cell was obtained. Conversion efficiency of 10% and 8.4% were obtained for $CH_3NH_3GeI_3$ and $CH_3NH_3GeBr_3$ respectively.

***Keywords*:** $CH_3NH_3GeI_3$, $CH_3NH_3GeBr_3$, DFT, FHI-aims, Energy-band gap, lattice constant, total energy, dielectric constants, linear-thermal-expansion-coefficient and Conversion Efficiency.

1. Introduction

The research into new types of solar cells is driven by the need for cheaper, clean and sustainable energy. One promising route for departing from the traditional solar cells is the dye-sensitized solar cell (DSSC). In this type of cell, the light is harvested by a sensitizer, which may be

a dye molecule or a semiconductor quantum dot attached to a wide-band-gap semiconductor of Nano-crystalline morphology, typically TiO_2 [1]. Dye-sensitized solar cells have stood out among various photovoltaic devices owing to their low cost, simple fabrication procedure, environmental friendliness, and relatively high efficiency. Consequently, DSSCs are promising candidates for the next generation solar cells [2]. The research into new types of solar harvesters for solar cells is driven by the need increase their efficiency and make them more reliable. One promising material for replacing the dye molecule solar harvesters is the organic–inorganic hybrid perovskite. One of the backdrops of dye-molecule harvesters is the fact it exists in liquid form and can dry up unlike the organic-inorganic hybrid perovskites which are in solid form. The introduction of organic–inorganic hybrid perovskites materials as light harvesters and charge carrier transporters; has improve the solar conversion efficiency of DSSCs; such DSSCs are called Perovskites Solar cells (PSC) or Solid-State Dye Sensitized Solar cells (SSDSC). Typically, the light-harvesting active layer is a hybrid organic-inorganic lead or tin halide-base material, the popular among is being methyl ammonium lead iodide, $CH_3NH_3PbI_3$ [3]. Perovskite materials such as the methyl ammonium lead halides are cheap to produce and simple to manufacture. Solar cell efficiencies of devices using these materials have increased from 3.8% in 2009 [4] to a certified 20.1% in 2014, making this the fastest-advancing solar technology [3]. According to detailed balance analysis, the efficiency limit of perovskite solar cells is about 31%, which approaches the Shockley-Queisser of gallium arsenide which is 33% [5].Their high efficiencies and low production costs make perovskite solar cells a commercially attractive option. Although methyl ammonium lead iodide, ($CH_3NH_3PbI_3$) has proven to be an effective active layer material, there remains a main concern about the toxicity of lead. Lead-based perovskites are a major issue that may prejudice implementation of any PSC technology, both regulation and common sense suggest that PSCs have to become lead free to deliver a sustainable technology [6]. Given the above developments, the determination of a lead free halide perovskite is of outstanding interest.

To design an efficient solar cell device, a deep understanding of underlying material's properties such as chemical composition, mechanical, electrical, and optical properties are required. Quantum mechanical approaches provide a deep understanding of properties of many body systems such as chemical composition, mechanical, electrical, and optical properties. Among the large panel of available theoretical approaches, the density-functional theory (DFT) has become overwhelmingly popular. Its success greatly relies on the existence of efficient computer numerical codes. In these numerical codes the input parameters can be adjusted. The overall principles of DFT are based on the Hohenberg–Kohn's theorems [7]. DFT has a strong versatility especially in the description of the ground state properties of semiconductors and metals. Increase in computing power has afforded further capabilities in system's size that DFT methods can handle.

In this work, an investigation into the possible replacement of $CH_3NH_3PbI_3$ with $CH_3NH_3GeI_3$ and $CH_3NH_3GeBr_3$ as the active layer in perovskite solar cell. The band structure analysis and energy bandgap calculation was performed. An investigation into the effect of

temperature on lattice constant (lattice expansion) and the effect of lattice constant (lattice expansion) on energy bandgap of the materials was carried out. Furthermore, the dielectric constant was determined.

2.0 Methodology

In this work ab-initio calculation in the framework of density functional theory DFT, as implemented in the FHI-aims package was performed [8]. The geometries of $CH_3NH_3GeI_3$ and $CH_3NH_3GeBr_3$ were built from the structural parameter obtained from existing literature[9] using Visualization for Electronic and Structural Analysis (VESTA) [10] and Avogadro software [11]. The generalized gradient approximation GGA with the blyp parameterization was employed for the evaluation of the exchange-correlation energy. Optimization of the followings configuration parameters; *occupation type (Gaussian or Fermi), charge mix param, initial moment, and n max pulay* was also performed. The Gamma-centered grid method has been chosen for sampling the Brillion zone. Full relaxation of the atomic positions within the unit cell was performed following the Broyden-Fletcher Goldfarb-Shanno (BFGS) optimization algorithm. Optimal lattice constant was also determined for each structure. The **k**-paths ($\Gamma - X - M - \Gamma - R - X|M - R$)[12]was used in the band structure analysis. Energy band gap were calculated for the optimized geometries along with the optimized configuration parameters using the FHI-aims code. The next procedures was only performed for those materials that gave a promising energy band gap.

To determine of how the vibrational band structures and the associated free energies, change with the volume of materials. The optimal lattice constant of the materials were determined by finding the minimum of the total energy $E_{DFT}(V)$ and $F^{ha}(T,V)$ by using the Birch-Murnaghan's equation of state[13]. Though, in the canonical ensemble, the relevant thermodynamic potential that needs to be minimized is the free energy $F(T,V)$ which is given by:

$$F(T,V) = E_{DFT}(V) + F^{ha}(T,V) \qquad (12)$$

To account for the volume dependence of $F(T,V)$, the total energy, $E_{DFT}(V)$ and free energy, $F^{ha}(T,V)$ were calculated for a series of lattice constants. Eq. (12) was then evaluated and minimized using the Birch-Murnaghan's Equation of states, the phonopy program package and its FHI-aims interface phonopy-FHI-aims are used here. A FHI-aims python script titled: *Compute_ZPE_and_lattice_expansion.py* [14] is used to perform the above procedure, this script requires the following inputs; optimal (equilibrium) lattice constant, the temperature range (0 to 350*K*) and geometry information. The script gives two output files; one contains temperature, the lattice constant and the lattice expansion coefficient and the other contains the equilibrium lattice constant computed with and without zero point energy (ZPE).and bulk modulus.

The investigation of the temperature dependence of the electronic band gaps of materials was carried out using a second python script titled: *Compute_bandgap_at_different_volumes.py*. Here electronic band structure calculations were performed for geometries constructed using the lattice constants generated from by the first script for temperature range of 273 to 318 *K*. This script

gives an output file that contains both the lattice constants and the energy bandgap as a function of temperature. To obtain the linear dielectric tensor in FHI-aims the tag *compute_dielectric* is used. It calculates and output the component of the imaginary and real part of the inter-band and intra-band contribution to the linear dielectric tensor.

A numerical simulation was carried out using these materials as the active layer in a perovskite solar cell, this was achieved by the use of General-purpose Photovoltaic Device Model (GPVDM). GPVDM is a free general-purpose tool for simulation of light harvesting devices. The model solves both electrons and holes drift-diffusion, and carrier continuity equations in position space to describe the movement of charge within the device. The model also solves Poisson's equation to calculate the internal electrostatic potential. The software gives an output that contains the Current-Voltage (I-V) characteristic curves [15]. The simulation was run for an active layer thickness of $3 \times 10^{-7} m$ and device temperature of 330 K.

3.0 Results and Discussion

3.1 Lowest unoccupied molecular orbital (LUMO), Highest occupied molecular orbital (HOMO)and Bandgap

The LUMO, HOMO and bandgap calculated is tabulate below along with reported values where available. The LUMO level for $CH_3NH_3GeI_3$ is above the CBE of most anode materials (e.g. TiO_2 and SiO_2), this indicate that it can serve as good active layers, $CH_3NH_3GeBr_3$ on the other hand show good promise as its LUMO level is just below that of the anode materials. The bandgap of $CH_3NH_3GeI_3$ obtained in this work (i.e.1.606 eV)is close to the reported bandgap range for $CH_3NH_3PbI_3$; 1.662 eV [16] and 1.61 eV [17].The bandgap obtained for $CH_3NH_3GeI_3$in this work is 4.29 % higher than the reported value of 1.54 eV [18]. Figures 1(a) and1 (b) shows that the band gaps of materials increase with increasing lattice parameter like in most perovskite materials, contrary to most general semiconductors like Si and GaAs [16].

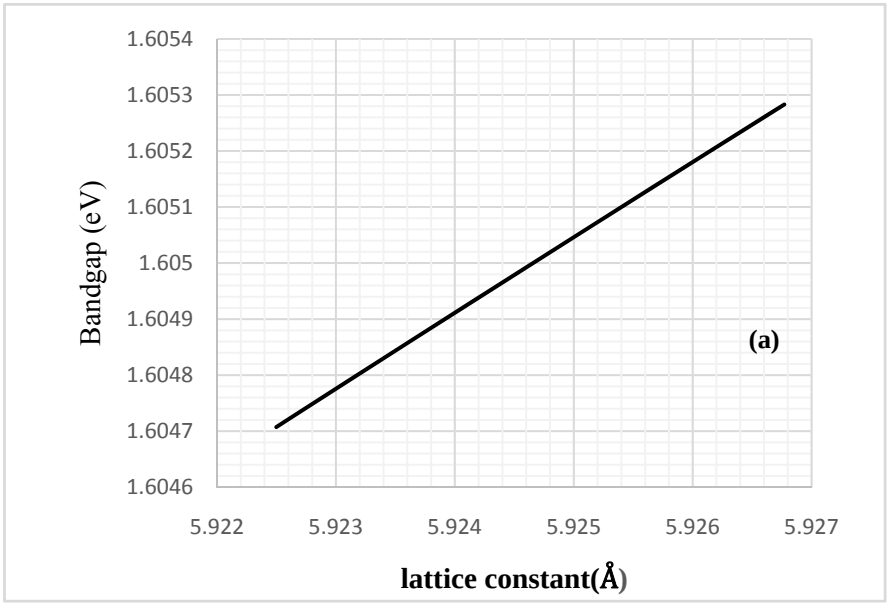

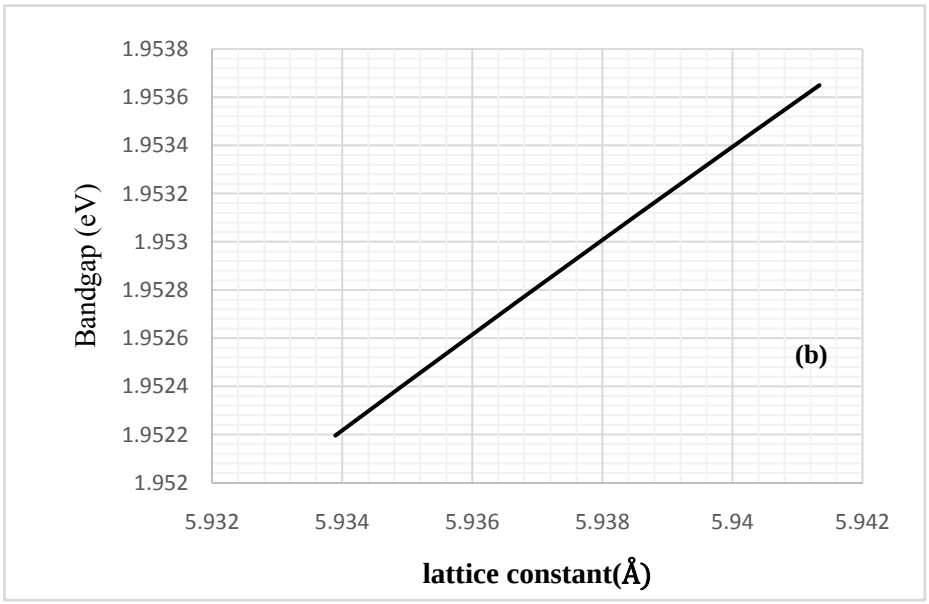

Fig. 1. Graph of bandgap against lattice constant for: (a) $CH_3NH_3GeI_3$ (b) $CH_3NH_3GeBr_3$

Table 1. LUMO, HOMO and Energy Band gap

Material	LUMO (eV)	HOMO (eV)	Band Gap (eV)	
			This work	Reported
$CH_3NH_3GeI_3$	-3.60616747	-5.21226324	1.606	1.54 [18] 2.0 [19]
$CH_3NH_3GeBr_3$	-3.85925193	-5.78400997	1.925	-

3.2 Lattice Constant

The lattice constants determined for each of the materials are listed in Table 2. There were little available data on lattice parameters of $CH_3NH_3GeI_3$and $CH_3NH_3GeBr_3$. Although the lattice constant obtained in this work was not compared with other reported values, the lattice constant increases from Br to I. A similar trend was found from Sn and Pb serials [16].

Table 2. Lattice Constant

Material	Lattice Constant(Å)		
	From Single point calculation	From phonopy without ZPE	From phonopy with ZPE
$CH_3NH_3GeI_3$	5.933	5.876	5.907
$CH_3NH_3GeBr_3$	5.833	5.877	5.894

3.3 Linear thermal expansion

Linear thermal expansion coefficient,α given in Eq. (11) was plotted against temperature for each of the materials, as shown in Figures 2(a), in figure 2(b) the same graph was plotted for more clarity for temperature range of 0 to 20 K. The change in lattice constant with temperature is shown in figure 2.Figure 2(a) shows that the linear thermal expansion coefficient does not change constantly with temperature, and it is negative for some very low temperatures, but in Figure 2(b) the negative expansion (contraction) can be seen to occur between the temperature ranges of 0 to 3 K. The temperature range at which the negative expansion occurs is the same for both materials. There is a constant increment of the expansion coefficient at temperatures above 3*K*. The negative expansion observed for this materials is similar to those observed in some semiconductors such as Germanium, Silicon, Diamond and Gallium Arsenide [20].The lattice constant expands with increase in temperature but with contraction at very low temperatures, this is obvious because of the negative linear thermal expansion observed in figure 2(b).

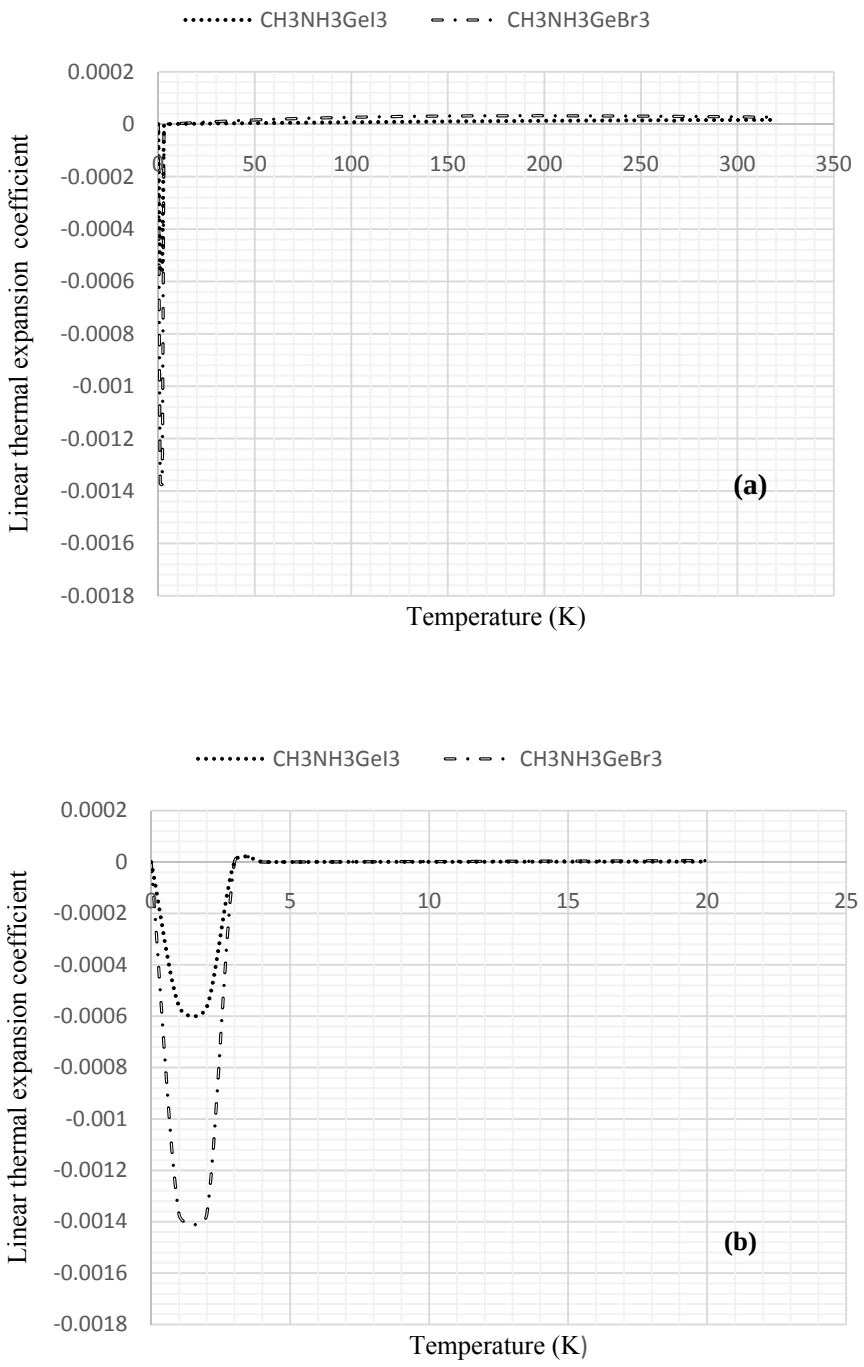

Fig. 2.Graph of Linear thermal expansion coefficient against temperature for: (a) $CH_3NH_3GeI_3$ (b) $CH_3NH_3GeBr_3$

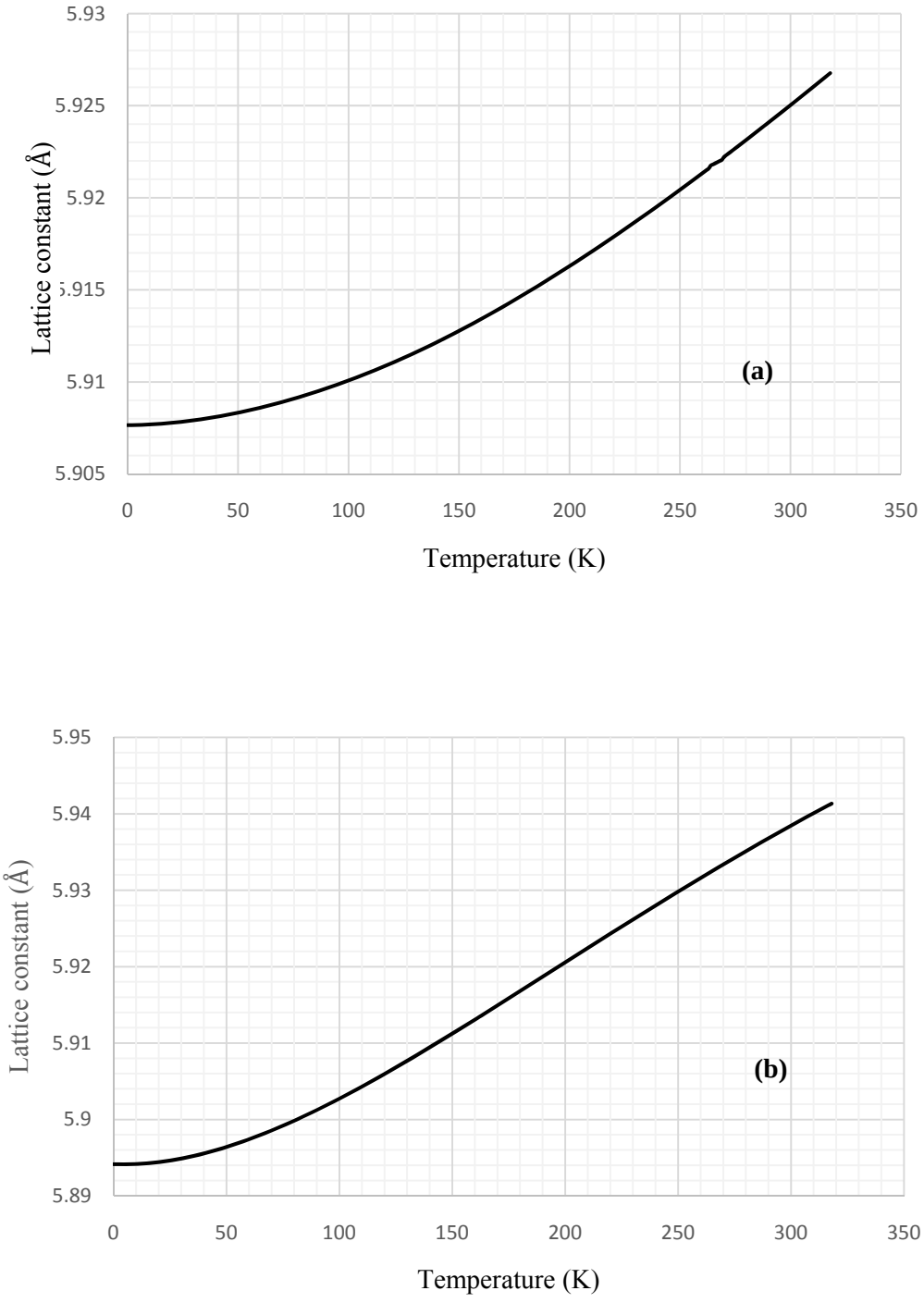

Fig.3 Graph of Lattice constant against temperature for: (a) $CH_3NH_3GeI_3$ (b) $CH_3NH_3GeBr_3$

3.4 Real components of dielectric Tensor

The graph of real components of linear dielectric tensor against frequency for cubic directions [100], [010], [001] and [111] are shown in figure 3(a) and 3(b). The dielectric constant (relative permittivity) which is value of the real part of the linear dielectric tensor at frequency equals to zero (i.e.$Re[\epsilon_r(\omega = 0)]$) for each of the above direction were given in Table 3.For both materials, the dielectric constant (relative permittivity) at the [100] and [010] directions have very close values, the ones obtained at [001] directions are higher than the ones at [100] and [010] directions. While the relative permittivity at the [111] direction has the highest value. The dielectric constant obtained at [111] direction for $CH_3NH_3GeI_3$(5.79) is close to the reported range of (5-7) [21] for $CH_3NH_3PbI_3$.

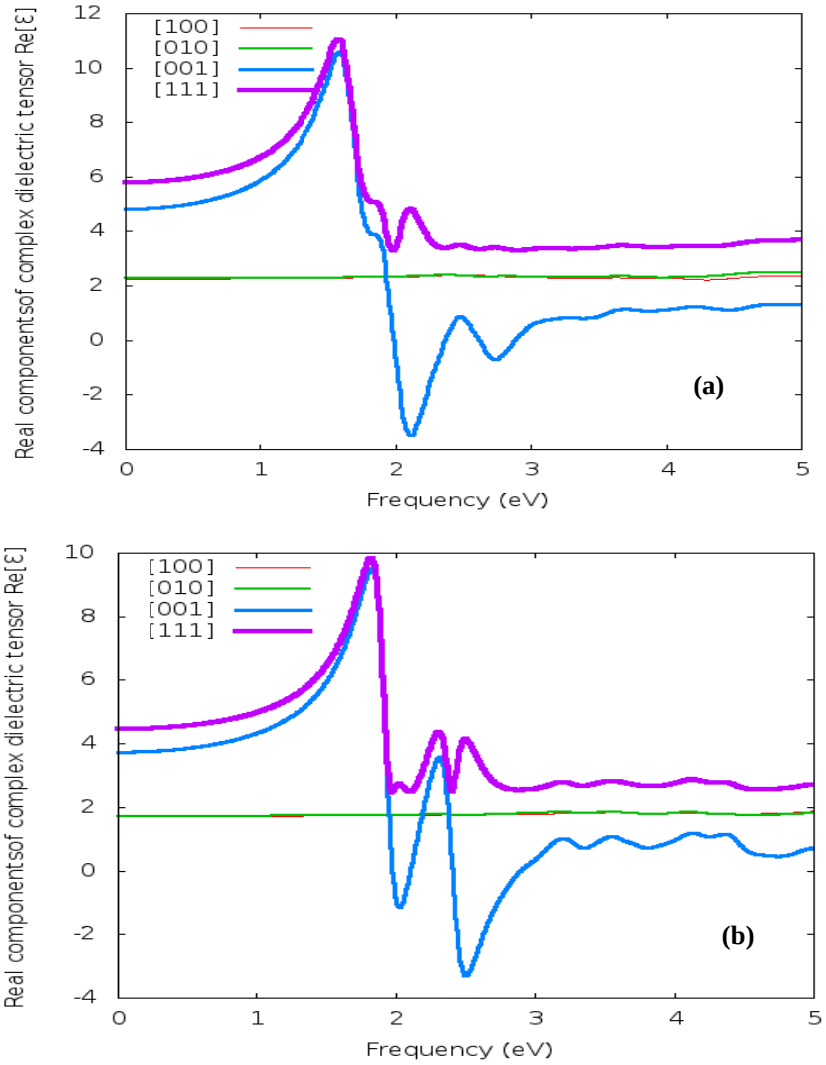

Fig. 4. Graph of real components of complex dielectric tensor against frequency for: (a) $CH_3NH_3GeI_3$ (b) $CH_3NH_3GeBr_3$

Table 3 Dielectric constant (ϵ)

Material	$Re[\epsilon_r(\omega = 0)]$			
	[100]	[010]	[001]	[111]
$CH_3NH_3GeI_3$	2.26	2.27	4.83	5.79
$CH_3NH_3GeBr_3$	1.72	1.72	3.73	4.46

3.5 Current-Voltage (I-V) Characteristic Curves

Current-Voltage (I-V) characteristic curves shown in figure 5 were obtained from the GPVDM software by using each of the material as the active layer in a perovskite solar cell. The current and voltage characteristics of a particular photovoltaic cell gives a detailed description of its solar energy conversion ability and efficiency. Knowing the electrical I-V characteristics of a solar cell is important in determining the device's output performance and solar efficiency. The maximum point voltage (V_{mp}) and maximum point current (I_{mp}) are deduced from the **Current-Voltage (I-V) characteristic Curves** for each of the materials, subsequently the maximum power point and efficiency were calculated these are shown in Table 4.

Table 4 Solar cell parameters

Material	V_{mp} (V)	I_{mp}(A)	Maximum power point (MPP) $MPP = V_{mp} \times I_{mp}$	Conversion Efficiency(η)(%) $\eta = \frac{MPP}{1000watts} \times 100\%$
$CH_3NH_3GeI_3$	0.5	200	100	10
$CH_3NH_3GeBr_3$	0.56	150	84	8.4

The conversion efficiency (η) of $CH_3NH_3GeI_3$ in this work was found to be higher than that of $CH_3NH_3GeBr_3$. The conversion efficiency for$CH_3NH_3GeI_3$and $CH_3NH_3GeBr_3$arelower than that of $CH_3NH_3PbI_3$ (14.4%) [22] by 30.5% and 41.6% respectively.

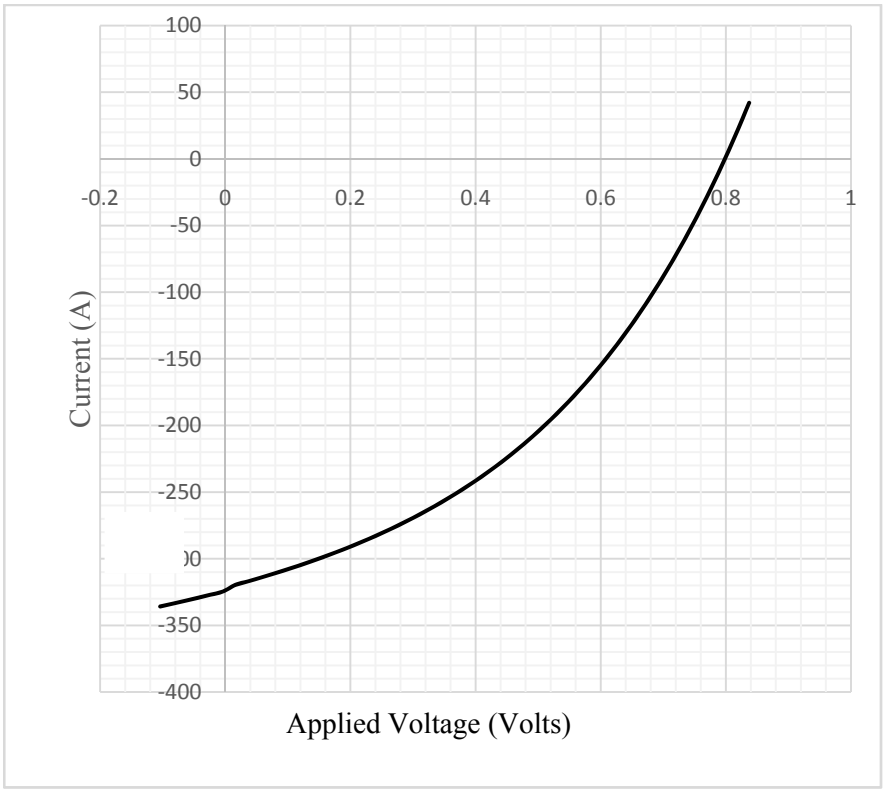

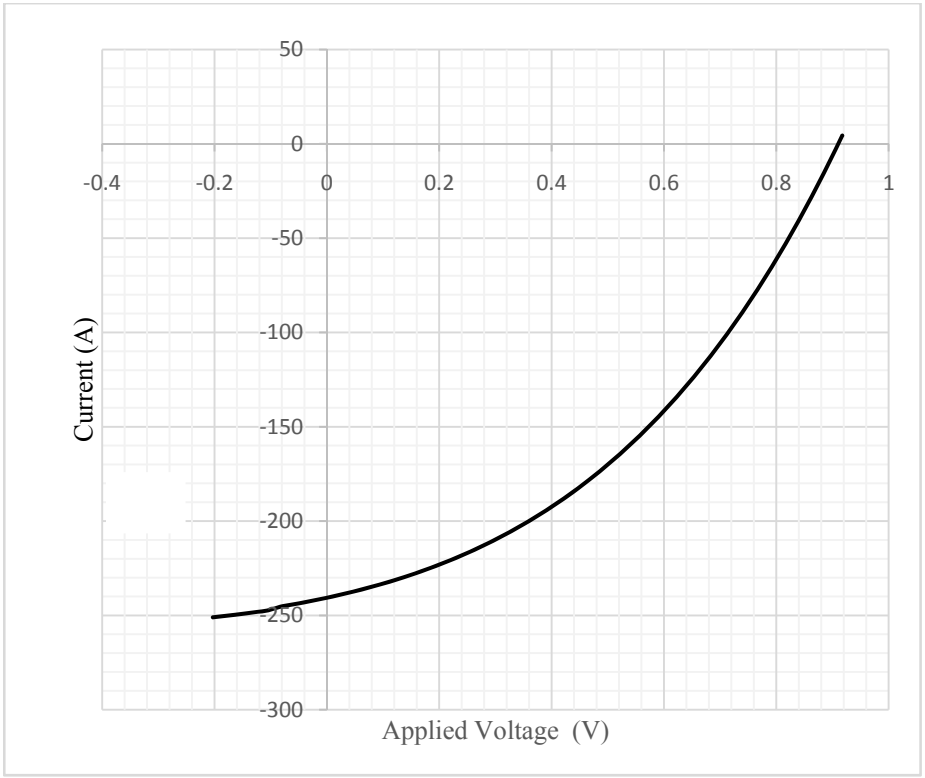

Fig.5. Current-vintage (I-V) curve using each of the materials as the active layer for: (a) $CH_3NH_3GeI_3$ (b) $CH_3NH_3GeBr_3$

4.0 Conclusion

All the calculations done in this work were based on Density Functional Theory method as implemented in FHI-aims code. FHI-aims code input parameters were optimized before the actual calculation and estimation were done. The bandgap of $CH_3NH_3GeI_3$ calculated in this work differ from reported result by 4.29 %, the band gaps of materials increase with increasing lattice parameter like in most perovskite materials. The trend observed in the lattice constant of $CH_3NH_3GeI_3$ and $CH_3NH_3GeBr_3$ is similar to that observed in other perovskite materials. Also the phonopy program package and its FHI-aims interface correctly predict the effect of temperature on linear thermal expansion coefficient and lattice constants of the materials, here the temperature dependence observed agrees with other established views. The conversion efficiency obtained gives an indication that these materials can be a good active layer candidate in perovskite solar cells. This can be verified further with an experimental work on these materials.

References

[1] Sarkar S. K., Hodes G., Kronik L. and Cohen H., Defect-dominated charge transport in Si-supported CdSe nanoparticle films. *The Journal of Physical Chemistry C,* 2008. **112**(16): p. 6564-6570.

[2] Yuan. S, Tang Q., Hu B., Ma C., Duan J and He B. Efficient quasi-solid-state dye-sensitized solar cells from graphene incorporated conducting gel electrolytes. *Journal of Materials Chemistry A*, 2014. **2**(8): p. 2814-2821.

[3] Völker, S.F., S. Collavini, and J.L. Delgado, Organic charge carriers for perovskite solar cells. *Chem Sus Chem,* 2015. **8**(18): p. 3012-3028.

[4] Kojima, A., Teshima, K., Shirai, Y and Miyasaka, T., Organometal halide perovskites as visible-light sensitizers for photovoltaic cells. *Journal of the American Chemical Society*, 2009. **131**(17): p. 6050-6051.

[5] Sha Wei EI, Ren, Xingang, Chen Luzhou and Choy Wallace CH, The efficiency limit of $CH_3NH_3PbI_3$ perovskite solar cells. *Applied Physics Letters,* 2015. **106**(22): p. 221104.

[6] Abate, A., Perovskite Solar Cells Go Lead Free. *Joule*, 2017.

[7] Arbuznikov, A., Hybrid exchange correlation functionals and potentials: Concept elaboration. *Journal of Structural Chemistry*, 2007. **48**: p. S1-S31.

[8] Blum, V., Gehrke, R., Hanke, F., Havu, P., Havu, V., Ren, X., Reuter,K. and Scheffler, M., Ab initio molecular simulations with numeric atom-centered orbitals. *Computer Physics Communications,* 2009. **180**(11): p. 2175-2196.

[9] Oku, T., Crystal structures of $CH_3NH_3PbI_3$ and related perovskite compounds used for solar cells, *Solar Cells-New Approaches and Reviews.* 2015, InTech.

[10] Momma, K. and F. Izumi, VESTA: a three-dimensional visualization system for electronic and structural analysis. *Journal of Applied Crystallography,* 2008. **41**(3): p. 653-658.

[11] Hanwell, M. D., Curtis, D. E., Lonie, D. C., Vandermeersch, T., Zurek E. and Hutchison, G. R.,Avogadro: an advanced semantic chemical editor, visualization, and analysis platform. *Journal of cheminformatics,* 2012. **4**(1): p. 17.

[12] Setyawan, W. and S. Curtarolo, High-throughput electronic band structure calculations: Challenges and tools. *Computational Materials Science,* 2010. **49**(2): p. 299-312.

[13] Franz, K. and L. Sergey, Tutorial II: Periodic Systems Manuscript for Exercise Problems: Presented at the Hands-on Tutorial Workshop on ab Initio Molecular Simulations at Fritz-Haber-Institut der Max-Planck-Gesellschaft Berlin. 2013, August.

[14] Christian, C., Tutorial IV: Phonons, Lattice Expansion, and Band-gap Renormalization Manuscript for Exercise Problems: Presented at the Hands-on Tutorial Workshop on ab Initio Molecular Simulations at Fritz-Haber-Institut der Max-Planck-Gesellschaft Berlin. 2015, July.

[15] MacKenzie, R. C., Kirchartz, T., Dibb, G. F. A and Nelson, J.*,* Modeling nongeminate recombination in P3HT: PCBM solar cells. *The Journal of Physical Chemistry C*, 2011. **115**(19): p. 9806-9813.

[16] Yuan, Ye Xu, Run, Xu, Hai-Tao Hong, Feng Xu, Fei and Wang, Lin-JunNature of the band gap of halide perovskites ABX_3(A= CH_3NH_3,Cs; B = Sn, Pb; X= Cl, Br, I): First-principles calculations. *Chin. Phys. B* 2015. **24**(11): p. 5.

[17] Heyd, J., G.E. Scuseria, and M. Ernzerhof, Hybrid functionals based on a screened Coulomb potential. *The Journal of Chemical Physics,* 2006. **118**(18): p. 8207-8215.

[18] Yuqiu, J., Yuanyuan, L. J., Li Mang, N. and Zhenqing, Y.,Exploring electronic and optical properties of $CH_3NH_3GeI_3$ perovskite: Insights from the first principles. *Computational and Theoretical Chemistry,* 2017. **1114**: p. 20-24.

[19] Hoefler, S.F., G. Trimmel, and T. Rath, Progress on lead-free metal halide perovskites for photovoltaic applications: a review. *Monatsh Chem,* 2017. **148**(5): p. 795-826.

[20] Dolling, G. and R. Cowley, The thermodynamic and optical properties of germanium, silicon, diamond and gallium arsenide. *Proceedings of the Physical Society,* 1966. **88**(2): p. 463.

[21] Park, N.-G., Methodologies for high efficiency perovskite solar cells. *Nano convergence,* 2016. **3**(1): p. 1-13.

[22] Abdulsalam, H., G. Babaji, and H.T. Abba, The Effect of Temperature and Active layer thickness on the Performance of CH3NH3PbI3 Perovskite Solar Cell: A Numerical Simulation Approach. *Journal for Foundations and Applications of Physics,* 2018. **5**(2): p. 141-151.